(1989) J. Mol. Biol. 209, 459-474.
Garrett-Wheeler, E., Lockard, R. E., & Kumar, A. (1984) Nucleic Acids Res. 12, 3405-3423.
Gutell, R. R. & Woese, C. R. (1990) Proc. Natl. Acad. Sci. U.S.A. 87, 663-667.
Happ, C. S., Happ, E., Nilges, M., Gronenborn, A. M., & Clore, G. M. (1988) Biochemistry 27, 1735-1743.
Haselman, T., Camp, D. G., & Fox, G. E. (1989) Nucleic Acids Res. 17, 2215-2221.
Jaeger, J. A., Turner, D. H., & Zuker, M. (1989) Proc. Natl. Acad. Sci. U.S.A. 86, 7706-7710.
Kim, S. H., Quigley, G. J., Suddath, F. L., McPherson, A., Sneden, D., Kim, J. J., Weinzierl, J., & Rich, J. (1973) Science 179, 285-288.
Levitt, M. (1969) Nature (London) 224, 759-763.
Metzler, W. J., Hare, D. R., & Pardi, A. (1989) Biochemistry 28, 7045-7052.
Moras, D., Comarmond, M. B., Fischer, J., Weiss, R., Thierry, J. C., Ebel, J. P., & Giegé, R. (1980) Nature (London) 288, 669-674.
Ninio, J., Favre, A., & Yaniv, M. (1969) Nature (London) 223, 1333-1335.
Saenger, W. (1984) in Principles of Nucleic Acid Structure, Springer-Verlag, New York.
Sampson, J. R., DiRenzo, A. B., Behlen, L. S. & Uhlenbeck, O. C. (1989) Science 243, 1363-1366.
Schevitz, R. W., Podjarny, A. D., Krishnamachari, N., Hughes, J. J., Sigler, P. B., & Sussman, J. L. (1979) Nature (London) 278, 188-190.
Shimmel, P. R., & Redfield, A. G. (1980) Annu. Rev. Biophys. Bioeng. 9, 181-221.
Srinivasan, A. R., & Olson, W. K. (1987) J. Biomol. Struct. Dyn. 4, 895-938.
Sussman, J. L., Holbrook, S. R., Warrant, R. W., Church, G. M., & Kim, S.-H. (1978) J. Mol. Biol. 123, 607-630.
Tinoco, I., Jr., Borer, P. N., Dengler, B., Levine, M. D., Uhlenbeck, O. C., Crothers, D. M., & Gralla, J. (1973) Nature (London), New Biol. 246, 40-41.
Woo, N. H., Roe, B. A., & Rich, A. (1980) Nature (London) 286, 346-351.
Wright, H. T., Manor, P. C., Beurling, K., Karpel, R. L., & Fresco, J. (1979) in Transfer RNA: Structure, Properties, and Recognition, Cold Spring Harbor Monograph Series 9A, pp 145-160, Cold Spring Harbor Laboratory, Cold Spring Harbor, NY.
Yaniv, M., Favre, A., & Barrell, B. G. (1969) Nature (London) 223, 1331-1333.
Zachau, H. G., Dutting, D., Feldman, H., Melchers, F., & Karau, W. (1966) Cold Spring Harbor Symp. Quant. Biol. 31, 417-424.

Molecular Dynamics Investigation of the Interaction between DNA and Distamycin†

K. Boehncke, M. Nonella, and K. Schulten*
Beckman Institute and Department of Physics, University of Illinois, 405 North Mathews Avenue, Urbana, Illinois 61801
A. H.-J. Wang
Beckman Institute and Department of Physiology and Biophysics, University of Illinois, 524 Burrill Hall, Urbana, Illinois 61801
Received August 20, 1990; Revised Manuscript Received January 4, 1991

ABSTRACT: The complex of the minor groove binding drug distamycin and the B-DNA oligomer d-(CGCAAATTTGCG) was investigated by molecular dynamics simulations. For this purpose, accurate atomic partial charges of distamycin were determined by extended quantum chemical calculations. The complex was simulated without water but with hydrated counterions. The oligomer without the drug was simulated in the same fashion and also with 1713 water molecules and sodium counterions. The simulations revealed that the binding of distamycin in the minor groove induces a stiffening of the DNA helix. The drug also prevents a transition from B-DNA to A-DNA that was found to occur rapidly (30 ps) in the segment without bound distamycin in a water-free environment but not in simulations including water. In other simulations, we investigated the relaxation processes after distamycin was moved from its preferred binding site, either radially or along the minor groove. Binding in the major groove was simulated as well and resulted in a bound configuration with the guanidinium end of distamycin close to two phosphate groups. We suggest that, in an aqueous environment, tight hydration shells covering the DNA backbone prevent such an arrangement and thus lead to distamycin's propensity for minor groove binding.

Control of gene expression at the level of transcription is emerging as a central area of investigation in biology (Stryer, 1988). The availability of respective DNA sequences and of structures of regulatory proteins involved in this control will allow one to rationalize underlying mechanisms. For example, it is now well understood how a number of repressor proteins interact with their respective operator DNA sequences at the molecular level (Ptashne, 1986). However, the structural complexity and large variability of regulatory protein-DNA interactions make it likely that structures of regulatory protein-DNA complexes will not be readily available. Therefore, molecular modeling and molecular dynamics may play an important role in combining information from various ex-

†M.N. gratefully acknowledges financial support by the Kanton Zürich, Switzerland. This work was carried out in the Center for Parallel Computation in Molecular Dynamics funded by the National Institute of Health. Computation time was granted by the National Center for Supercomputing Applications at the University of Illinois in Urbana-Champaign supported by the National Science Foundation.
*To whom correspondence should be sent.

0006-2960/91/0430-5465$02.50/0

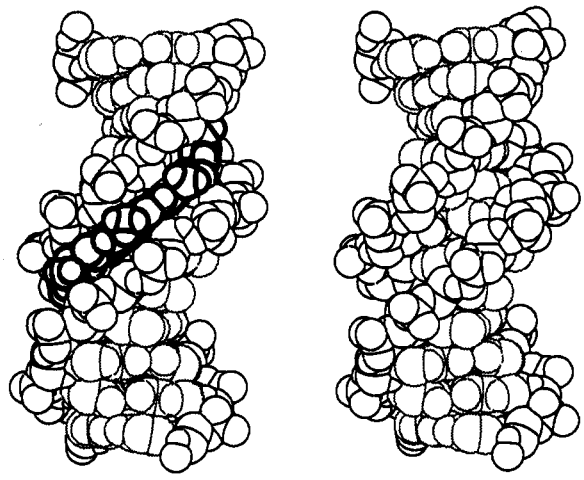

FIGURE 1: B-DNA segment consisting of 12 base pairs with the drug distamycin bound to the minor groove (left) and without the drug (right).

periments to describe the relevant structures at the level of detail needed to understand control mechanisms.

The method of molecular dynamics simulation of biopolymers is still in its infancy, and presently much effort is being spent toward achieving more faithful descriptions of molecular properties and achieving simulations of larger systems over longer time scales. The efforts involve the development of new simulation programs as well as new computer hardware (Heller et al., 1990; Windemuth & Schulten, 1990). Most developments of molecular dynamics methods have focused on improved descriptions of protein systems, since such systems were investigated by the majority of biochemists. The exciting prospects of the biochemistry of gene control, however, have lead to increased efforts spent on developing and calibrating molecular dynamics simulations of regulatory protein binding to DNA.

In this paper, we used molecular dynamics simulations to investigate a molecular complex involving the symmetric DNA oligomer d(CGCAAATTTGCG) and the drug distamycin. The three-dimensional structure of this complex has been determined by X-ray crystallography to 2-Å resolution (Coll et al., 1987) and has been compared to a similar complex of a DNA oligomer with netropsin (Coll et al., 1989). These complexes are much smaller than regulatory protein–DNA complexes and also involve binding in the minor groove rather than in the major groove, i.e., a different interaction motif than for regulatory proteins (Stryer, 1988). However, the small size permits a detailed molecular dynamics investigation.

Distamycin is known to bind in the minor groove in AT-rich regions of DNA, and its effect on DNA has been well characterized (Zimmer & Wahnert, 1986). Hence, the distamycin–DNA complex provides an ideal test case for the development of molecular dynamics simulations. The complex is shown in Figure 1. Ligand–DNA complexes previously simulated by molecular dynamics include the drugs actinomycin D (Creighton et al., 1989) and spermine (Feuerstein et al., 1989). In the case of distamycin, to our knowledge only molecular mechanics, i.e., a minimization technique, has been applied (Pelton & Wemmer, 1988). Our investigation focused on structural effects that distamycin might have on DNA. For example, it is known that the drug inhibits the transition from B- to A-DNA that results when DNA is dehydrated (Zimmer & Wahnert, 1986). We also attempted to characterize the binding of distamycin by moving the drug away from its binding position and by simulating rebinding. Additionally, we investigated the effect that water bound to the DNA might have on the drug–DNA interaction.

It must be noted at the outset that even for a complex as small as distamycin–d(CGCAAATTTGCG), with roughly 600 atoms, the possibilities for molecular dynamics simulations are very limited. The main reason is that faithful descriptions must involve counterions and a large number of water molecules and cover time scales that are presently unfeasible. In this paper, we present simulations that either involved the above-mentioned DNA segment in vacuo, together with 1713 water molecules, or involved only the DNA segment and distamycin. A full simulation of the binding of distamycin to DNA in the presence of water is prohibitive, since the process of replacing water by the drug is far too slow to be simulated. However, we found that simulations of DNA–water and DNA–drug systems together provide some interesting conclusions regarding the mechanism of binding.

METHODS

In this section we will briefly discuss the methodological problems encountered with molecular dynamics simulations of DNA and its complexes. We then consider distamycin's charge distribution and force field parameters and finally state in detail which simulations were carried out for the present investigation.

Molecular dynamics studies of DNA date back several years. The goal of the first simulations (Levitt, 1983; Tidor et al., 1983) was basically to examine if stable modeling of DNA systems by molecular dynamics could be achieved. Problems arose because of the accumulation of negative charges of the phosphate groups on the DNA backbone. The number of atoms and the resulting computational requirements only permitted simulations in vacuo, and in this medium the electrostatic forces cause DNA to unwind. Therefore, charges on the phosphate groups were either neglected (Levitt, 1983) or reduced (Tidor et al., 1983) while at the same time a distance-dependent dielectric was introduced to further weaken the electrostatic interactions. These modifications resulted in stable DNA strands. Singh et al. (1985) analyzed the effect of counterions on DNA structure and dynamics with fully charged phosphate groups and used a distance-dependent dielectric $\epsilon = r$ (Å) and positive, hexahydrated counterions. A stable DNA–counterion simulation was achieved, and sugar puckering angles were found to be in qualitative agreement with NMR studies. A serious problem of DNA dynamics simulations is a comprehensive representation of the huge amount of data, i.e., the conformational and helicoidal parameters of a double strand and their time evolution. A very detailed and elegant analysis of a 30-ps molecular dynamics study on a dodecamer double helix has been presented by Ravishanker et al. (1989).

In order to obtain a more realistic description of DNA dynamics, it became necessary to further improve upon the representation of water. One of the first molecular dynamics simulations of DNA and water was carried out by van Gunsteren et al. (1986) with the aim of comparing simulation results with 2-D NMR data. The modeling was successful, with 80% of the NOE distances reproduced within experimental error. Interestingly, structural changes were observed in the DNA segment. Even though the simulation began with a B-DNA structure, it ended with a hybrid of about 70% B-DNA and 30% A-DNA.

Molecular dynamics simulations of biopolymers require a knowledge of force field parameters and atomic partial charges of all components, e.g., of DNA strand and drug or of water. For many proteins with their respective prosthetic groups and for nucleic acids, such force fields have been developed (Weiner

et al., 1986; Nilsson & Karplus, 1986; Brooks et al., 1983). We have based our investigation on the force field of the molecular dynamics program CHARMM (Brooks et al., 1983). This force field has been developed and applied mainly in the context of proteins, and its DNA parameters are not as well tested as the parameters for proteins.

For the present study, a force field and atomic partial charges of distamycin were required. It had been suggested that, in addition to electrostatic forces, interactions due to hydrogen bonding and van der Waals contacts are responsible for the site specificity of distamycin binding (Wang & Teng, 1990). The issue is of considerable importance, since it may explain if distamycin recognizes AT-rich sections in the minor groove of DNA as a "lock and key" template, an electrostatic template, or a combination of both [for a review of drug specificity see Hurley (1989)]. In order to gauge electrostatic contributions to distamycin binding, we considered it to be important to carry out simulations with accurate atomic partial charges. In the following section we will discuss how such charges have been determined.

Charge Distribution for Distamycin

Partial charges of distamycin employed in the molecular mechanics study (Pelton & Wemmer, 1988) were obtained according to the semiempirical MNDO method (Dewar & Thiel, 1977). However, such charges are known to depend sensitively on the semiempirical method used (Smeyers et al., 1988). Therefore, we carried out a set of quantum chemical ab initio calculations in order to obtain a new set of charges and to estimate their accuracy.

An important aspect for calculations of partial atomic charges is the choice of a criterion necessary for assigning electron density to atomic centers. The procedure used most often is that of Mulliken (1955), which is computationally simple but strongly dependent on the basis set. In particular, the method is not suitable for extended basis sets required for an adequate description of the electronic structure of molecules. Therefore, we employed a procedure proposed by Davidson (1967) and Roby (1974) and further developed by Heinzmann and Ahlrichs (1976). This method yields results that are less dependent on variations in basis sets than the Mulliken method. In the Roby–Davidson method, the converged SCF wave function is first transformed into a minimal basis set of modified atomic orbitals (MAO's). By use of the one-particle density operator, occupation numbers of these MAO's are calculated. Population analysis that assigns partial charges is then based on these occupation numbers.

Distamycin consists of 63 atoms, which is very large for typical ab initio calculations. In order to render the calculation of atomic partial charges involving larger basis sets more feasible, we adopted the following procedure, schematically presented in Figure 2, parts a and b. We reduced the size of the drug from 63 to 48 atoms by removing the second of the three pyrrole rings. The atomic partial charges for the smaller molecule were then evaluated as explained in the following paragraph. Next, the charge distribution of the complete distamycin was extrapolated from the reinsertion of the removed pyrrole ring and the subsequent adoption of the charge distribution for this ring from that of the other two rings (shaded regions in Figure 2, parts a and b). The charge distribution of the three rings was then rescaled to conserve a total charge of +1 for the entire molecule.

The coordinates for the drug that were used in our quantum chemical calculations were taken from the X-ray coordinates of the distamycin–B-DNA complex (Coll et al., 1987). The Hartree–Fock wave function of the fully charged smaller

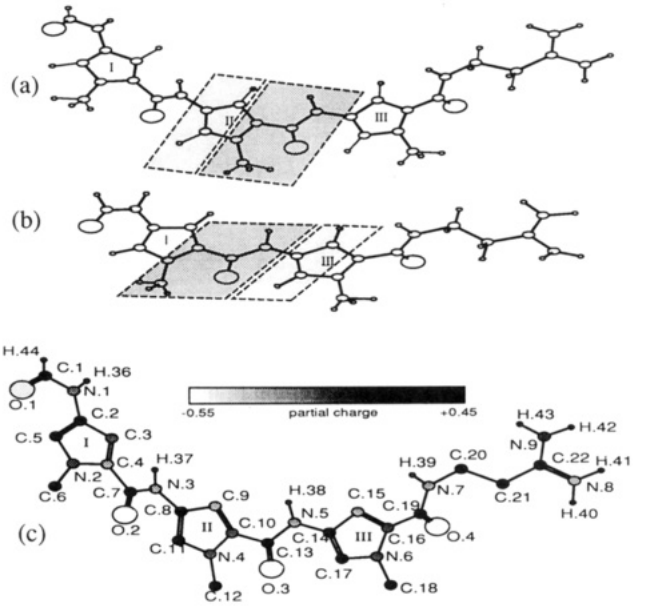

FIGURE 2: (a) Distamycin molecule. (b) Smaller version of distamycin after ab initio calculations were performed to determine its charge distribution. The charge distribution for ring II of the complete molecule was taken from the pertinent shaded regions of the smaller molecule. (c) Distamycin with polar hydrogens and the charge distribution used in the simulations.

molecule (see Figure 2b was calculated by use of a direct SCF program written by Häser and Ahlrichs (1989). To test the basis set dependence of the resulting charge distribution, we employed several basis sets: a Huzinaga MINI basis set (Huzinaga et al., 1984), leading to 152 contracted basis functions; a Huzinaga MIDI basis set (Huzinaga et al., 1984), leading to 278 basis functions; a double-ζ (DZ) basis set (Huzinaga, 1971), leading to 304 contracted basis functions; and a double-ζ basis set with polarization functions (DZP), leading to 500 contracted basis functions. The exponents of the polarization functions were $\alpha_O = 1.25$, $\alpha_N = 0.8$, $\alpha_C = 0.7$, and $\alpha_H = 0.8$. To obtain partial charges from the resulting SCF wave functions, Mulliken and Roby–Davidson population analyses were performed. For the Roby–Davidson population analysis, one MAO for hydrogen and five MAO's for carbon, nitrogen, and oxygen were chosen. The charges of the nonpolar hydrogen atoms were incorporated into the corresponding heavy atoms.

For the overall variations of the atomic charges that we determined with the different basis sets, we obtained the following standard deviations: MINI → MIDI, 0.138 (Roby), 0.219 (Mulliken); MIDI → DZ, 0.041 (Roby), 0.096 (Mulliken); and DZ → DZP, 0.076 (Roby), 0.154 (Mulliken). The Roby–Davidson method, obviously, is less dependent on basis sets than the Mulliken population analysis. Furthermore certain atomic charges calculated according to the Mulliken method show unreasonably large values. In order to test the dependence of atomic charges on the semiempirical method applied, INDO (Pople et al., 1967) and AM1 (Dewar et al., 1985) calculations of the complete distamycin were carried out. The standard deviation obtained for the differences in atomic charges is 0.126 and, therefore, is comparable to the values obtained from the results of ab initio calculations with different basis sets. For our parametrization of distamycin we adopted atomic partial charges resulting from the largest basis set, the DZP basis set, and the Roby–Davidson method.

The resulting atomic partial charges, which are used in our molecular dynamics calculations, are depicted in Figure 2c. About 78% of distamycin's positive charge is located at the

CN_2H_4 group, leading to strong electrostatic interactions between the drug and the negatively charged phosphate groups of the DNA segment. This result is in good agreement with MNDO calculations (Pelton & Wemmer, 1988), which assign 83% of the positive charge to the terminal group. Our charge distributions differ from the one calculated with the MNDO method mainly in the region of the peptide bonds in that partial charges of the corresponding oxygen atoms are generally more negative by about 0.2–0.3 electron charge. Since the atomic charges of carbons and nitrogens do not vary as strongly, the charge distribution calculated by us mainly results in a stronger polarization of the C=O bond.

For the subsequent molecular dynamics simulations, force field parameters for distamycin were required as well. These parameters were derived from the protein parameters packaged with the program X-PLOR and adapted for use with distamycin.

Molecular Dynamics

The molecular dynamics program X-PLOR (Brünger, 1988; Brooks et al., 1983) was used for all simulations. The DNA force field parameters packaged with the programs and used by us are those of Nilsson and Karplus (1986). For polar hydrogens, the explicit hydrogen bond potential was employed. Nonpolar hydrogens were included through an extended atom representation. The total charge on each of the DNA phosphate groups was −1. A radius-dependent dielectric constant of $\epsilon(r) = r$ (Å) was used for the simulations that were done in vacuo without a cutoff of pair interactions. In the simulation with water and DNA, we employed TIP3 water molecules with angles and bonds constrained by the SHAKE algorithm (van Gunsteren & Berendsen, 1977), with a dielectric constant of $\epsilon = 1$ and with a cutoff of nonbonding interactions of 15 Å.

In all molecular dynamics runs, the SHAKE algorithm was used to fix the bond lengths involving hydrogen. The integration time step was 1 fs. The coordinates of all atoms were written out for analysis every 50 fs. Except for the heating and equilibration processes described below, all dynamics simulations assumed a *t*-coupling (Berendsen et al., 1984) term with $\beta = 0.2$ ps^{-1} and a bath temperature of 300 K.

The following simulations were carried out and will be referred to by the labels stated at the beginning of the definitions.

$DNA_{no\ dist}$: 240-ps simulation of the B-DNA segment d-(CGCAAATTTGCG) without distamycin. The starting structure was the (minimized, equilibrated) X-ray structure of Coll et al. (1987).

DNA_{water}: 27-ps simulation like $DNA_{no\ dist}$, but with a layer of explicit water molecules.

DNA_{dist}: 250-ps simulation of the B-DNA segment d-(CGCAAATTTGCG) with distamycin. The starting structure for the simulations was the (minimized, equilibrated) X-ray structure of Coll et al. (1987).

DNA_{ideal}: 250-ps simulation of an idealized B-DNA segment d(CGCAAATTTGCG) with distamycin. The simulation began with the (minimized, equilibrated) standard structure based on (Arnott & Hukins, 1972) least squares fitted to the X-ray structure. For distamycin, the same coordinates as in the X-ray structure were used.

$DNA_{move\,i}$: Simulation of DNA_{dist} with distamycin in several different starting positions (i = 1, 2, or 3) defined below in the minor and major grooves to investigate the characteristics of distamycin binding and the interaction of distamycin with the binding site. The starting configuration for these simulations was always the structure of the DNA moiety in the simulation DNA_{dist} (defined above) at 50 ps, i.e., at a time when the system had reached equilibrium with the heat bath. The distamycin molecule in this structure was moved to the desired starting position of the simulations. Counterions too close to this position were repositioned slightly. Both tasks were accomplished interactively with use of the graphics program Quanta (Polygen Corp., 1988). To prevent grossly unfavorable interactions at the new position, we subsequently performed a 40-step Powell minimization (Powell, 1977) of the distamycin molecule and the counterions that were moved. The energy function was minimized with respect to angle, dihedral, and van der Waals contributions. The simulations resumed by use of the *restart* file, which contained the velocities of all atoms prior to the repositioning of distamycin at the 50-ps mark. This ensured that the temperature would continue to be around 300 K. In the simulations $DNA_{move\,1}$–$DNA_{move\,3}$, distamycin had been moved away from its starting position, in the case of $DNA_{move\,1}$ radially by 4.1 Å, in simulation $DNA_{move\,2}$ along the groove by two base pairs, and in simulation $DNA_{move\,3}$ into the major groove. Other details of these simulations are described further below.

The initial DNA structures used in the simulations above were chosen as follows: In all simulations except DNA_{water}, DNA was surrounded by large "hexahydrated" positive counterions. These counterions, each modeled as suggested in Singh et al. (1985) with a charge of +1, a mass of 131.08 amu, and a van der Waals radius of 5 Å, were placed near the negatively charged phosphate groups at the O–O bisectors. In simulation $DNA_{no\ dist}$, 22 counterions were initially positioned at a distance of 8 Å from each phosphorus, ensuring electrical neutrality. In the structures with the positively charged distamycin (DNA_{dist} and DNA_{ideal}), 21 counterions were positioned at a distance of 12 Å from each phosphorus, a counterion near the phosphate group closest to the charged guanidinium end (atoms N8 and N9 in Figure 2c) of the drug being left out and charge neutrality being achieved through the charge of DNA_{dist}. In simulation DNA_{water}, 22 sodium ions were placed at a distance of 8 Å from each phosphorus and a layer 8–13 Å thick containing 1713 TIP3 water molecules was then added to the molecule by use of the program MODEL (Walberer, 1990). Because the original water molecules were placed on a cubic grid with a lattice constant of 3.05 Å in monooriented fashion, a 2-ps molecular dynamics simulation at 1000 K—fixing all DNA atoms and allowing only the water molecules to move—was run prior to minimization in order to randomize the water.

All simulations except those of the class DNA_{move} began with an energy minimization of the initial structure, a heating of the resulting structure, and equilibration. These steps will be described below.

For energy minimization we employed the Powell algorithm (Powell, 1977), calculating 500 steps. The resulting structures were then heated from 10 to 300 K by a molecular dynamics simulation with use of a stochastic heat bath modeled by a Langevin equation (Berkowitz & McCammon, 1982; Brooks et al., 1985). A friction coefficient of $\beta = 5$ ps^{-1} was used in the Langevin equation to ensure that the molecule would adapt to the temperature of the heat bath within about 0.5 ps. The bath temperature was raised by 25 K/ps, reaching 300 K after 12 ps. This heating method was employed, since we experienced structural variations with simpler procedures. Similar processes used for heating and cooling are described by Wong et al. (1989) and Tesch and Schulten (1990). The heating curves of all our systems are very similar; in each case the system temperature follows the bath temperature multistep function rather well, thus leading to a nearly linear temperature increase during the 12-ps heating interval.

Table I: Comparison of the Intramolecular Energies of the DNA during All Three Simulations[a]

energy (kcal/mol)	$DNA_{no\ dist}$	DNA_{ideal}	DNA_{dist}
angle	291.6 (11.9)	296.4 (11.7)	290.8 (11.9)
dihedral	240.6 (8.3)	251.5 (8.1)	244.7 (8.0)
bond	169.9 (9.6)	170.0 (9.4)	170.6 (9.1)
improper	63.0 (5.4)	67.8 (6.2)	65.7 (5.8)
electrostatic	−35.1 (10.3)	−44.6 (9.6)	−22.0 (8.5)
H bond	−60.1 (2.8)	−61.9 (3.4)	−56.8 (2.9)
van der Waals	−473.6 (7.5)	−478.7 (7.8)	−481.4 (8.7)
total	196.3 (14.5)	200.5 (16.5)	211.5 (19.1)

[a] The values listed were averaged over the final 200 ps of each simulation; the values in parentheses indicate the pertinent standard deviation.

After heating, all systems were equilibrated for 15 ps in a free dynamics run without coupling to an external bath. At the end of the equilibration run, all structures were at temperatures of around 320 K; in the case of the DNA_{water}, at a temperature of around 300 K.

Results and Discussion

In this section we provide an analysis of the configurational dynamics resulting from the various simulations described above. We focused our attention on the following properties: the average interaction energies, which provide a measure of the degree of equilibration, and the configurations of DNA and of distamycin relative to DNA.

Energy Analysis

At the start of a simulation, biopolymers are generally not in a relaxed, i.e., equilibrium, configuration with respect to the assumed force field. The configurational relaxation is accompanied by an exchange of energy between the degrees of freedon of the biopolymer; e.g., van der Waals energy is transformed into kinetic energy due to unfavorable sterical interactions. Monitoring the energies of the various degrees of freedom allows one to ascertain that a molecular system is well equilibrated. The interaction energies of a biopolymer also provide measures of molecular properties. The various forms of energy in a biopolymer system are defined in Brooks et al. (1983).

It should be recalled that in our simulations the atoms were in contact with a heat bath at 300 K through a *t*-coupling (Berendsen et al., 1983) term of $\beta = 0.2\ ps^{-1}$. All systems simulated required approximately 50 ps to attain equilibrium with the heat bath and to reach the target temperature of 300 K. In the following, we present only results obtained after an initial simulation period of 50 ps.

Analysis of the time development of the intramolecular DNA energy components in all simulations, i.e., DNA_{dist}, DNA_{ideal}, and $DNA_{no\ dist}$, shows that the various interaction energies are stable throughout the entire simulation of 250 ps. A slight decrease of the total energy is discernible only during the initial 50-ps period. This result is important in that it provides a firm basis for conclusions drawn from our simulations based on the assumption that the systems investigated are well equilibrated. The averaged energy values over the last 200 ps of the simulations are presented in Table I. The only energy contribution that shows a significant variation between the three simulations is the electrostatic energy. The variation can be accounted for by the drift of one of the counterions in the course of the DNA_{dist} simulation; the energy between counterions and DNA in the DNA_{dist} simulation is around 40 kcal/mol higher than the corresponding energy in the DNA_{ideal} simulation.

Table II: Mean Values and Standard Deviations of the Nonbonded Energies between DNA and Distamycin in Two Simulations

energy (kcal/mol)	DNA_{dist}	DNA_{ideal}
H bond	−15.3 (1.8)[a]	−15.6 (1.69)
van der Waals	−78.2 (3.6)	−81.4 (3.3)
electrostatic	−98.8 (4.9)	−103.8 (5.2)

[a] The values in parentheses indicate the pertinent standard deviation.

The nonbonded interaction energies between the DNA strand and distamycin are very stable both in the DNA_{dist} and in the DNA_{ideal} simulation. The energies corresponding to the final 50 ps of the DNA_{ideal} simulation are depicted further in the section Distamycin Binding (Figure 8a). The averaged nonbonded energies in the two simulations are listed in Table II. Again, as in Table I, there is no significant difference between the simulation DNA_{dist} begun from an X-ray structure and that (DNA_{ideal}) begun from the idealized model. This result is important because it implies that molecular dynamics simulations can be started from standard DNA structures rather than from observed X-ray structures. There are, however, two caveats: first, the simulation DNA_{dist} resulted in root-mean-square (rms) deviations significantly smaller than those in the simulation DNA_{ideal}, and second, the binding site of distamycin is only known from the X-ray structure. Simulation of binding involving optimal positioning along the minor groove is too time-consuming.

Structural Analysis

DNA transcription and replication require unwinding of the double helix and, hence, involve considerable flexibility and structural change. Therefore, it is of great interest to study how the binding of distamycin alters motional and structural properties of DNA. Such an effect could imply that the mechanism of distamycin may be a structural rigidification of DNA; however, the mechanism of distamycin's action is not known and might as well involve ternary drug–DNA–protein complexes (Hurley, 1989).

In the case of our study of a very short DNA segment, an interpretation of molecular dynamics results must discount trivial motions of the segment, i.e., translations and rotations. For this purpose, the trajectories pertaining to the final 200 ps of the three simulations DNA_{dist}, DNA_{ideal}, and $DNA_{no\ dist}$ were read one coordinate set at a time, each set least squares fitted to the respective starting structure by application of overall rotations and translations and averaged thereafter. In the fitting procedure, the base pairs at both ends of the DNA strand and the counterions were excluded because they have inherently large motional amplitudes and cannot be expected to stay aligned with the overall structures.

The starting and averaged structures of the $DNA_{no\ dist}$ and DNA_{dist} simulations are shown in Figure 3. The position of the bound distamycin is also indicated in Figure 3. An important motional property of the system is the rms deviation $\langle \Delta r_i^2 \rangle^{1/2}$ of each averaged atomic position

$$\langle \Delta r_i^2 \rangle^{1/2} = \sqrt{\frac{1}{N-1} \sum_{t=0}^{N} (|\mathbf{r}_{i,t} - \bar{\mathbf{r}}_i|)^2}$$

where N is the number of coordinate sets and i is the atom index. Here $\bar{\mathbf{r}}_i$ denotes the position of atom i averaged over the later 200 ps of the respective trajectories. In the isotropic harmonic model, these calculated mean-square atomic fluctuations are directly related to the experimental temperature factor B_i according to $B_i = {}^8/_3\pi^2\langle \Delta r_i^2 \rangle$. Calculated values of $\langle \Delta r_i^2 \rangle^{1/2}$ for both averaged structures are shown in Figure 3.

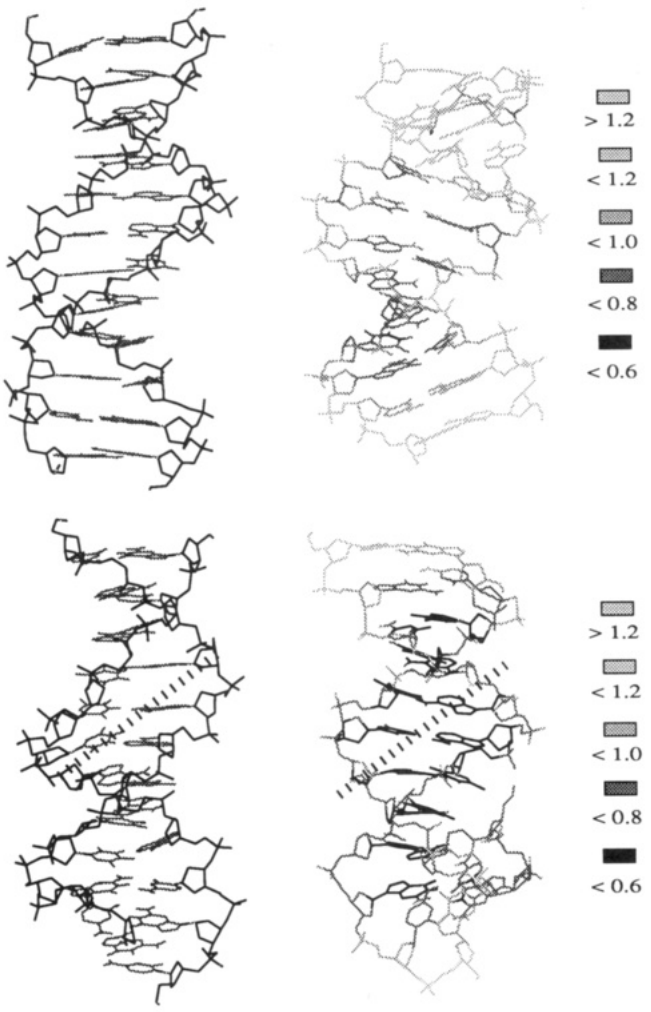

FIGURE 3: Stick representation of the starting $DNA_{no\ dist}$ structure (top, left) and its averaged structure (top, right) and of the starting DNA_{dist} structure (bottom, left) and its averaged structure (bottom, right). Both averaged structures are calculated from data taken during the final 200 ps of the simulation. Atomic mobilities (Å) are gray-coded in the averaged structures. The position of distamycin is indicated by the slanted lines.

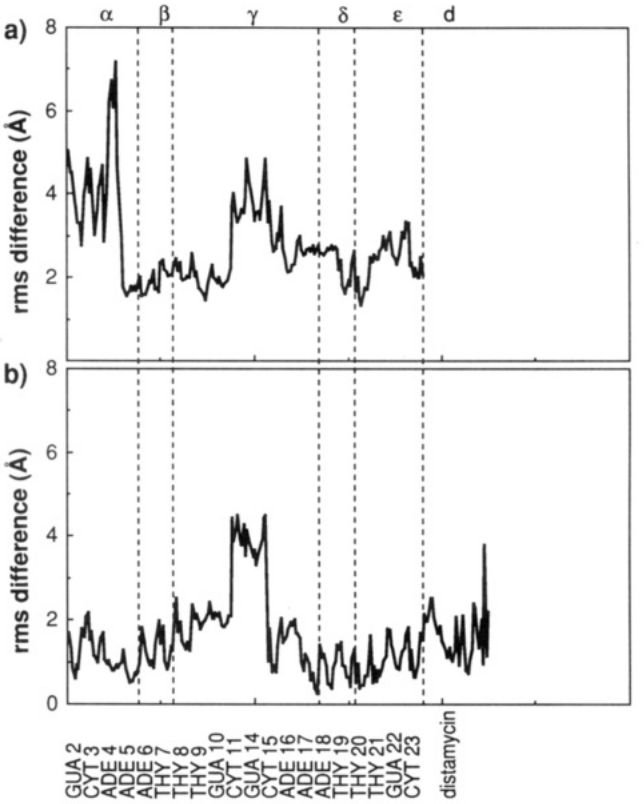

FIGURE 4: Deviation of non-hydrogen base-pair atoms from the original X-ray structure for the DNA segment without distamycin (simulation $DNA_{no\ dist}$) (a) and with distamycin (simulation DNA_{dist}) (b). The horizontal axis shows the base-pair atoms. The following regions are identified: (α) GUA 2 to ADE 5; (β) central base pairs ADE 6 and THY 7; (γ) THY 8 to CYT 11 (helix a) and GUA 14 to ADE 17 (helix b); (δ) central base pairs ADE 18 and THY 19; (ϵ) THY 20 to CYT 23; and (d) distamycin.

Table III: Propeller Twist Angles from X-ray and Averaged Structures

	X-ray structure		averaged structure	
base pair[a]	$DNA_{no\ dist}$	DNA_{dist}	$DNA_{no\ dist}$	DNA_{dist}
A(6)-T(19)	18.9	21.0	20.8	23.0
T(7)-A(18)	18.8	21.7	20.9	27.7

[a] Only the two central base pairs are listed.

A more detailed analysis of the atomic mobilities and a comparison with the experimental temperature factor for the structures $DNA_{no\ dist}$ and DNA_{dist} are presented in Figure 5. One can recognize clearly from a comparison of the two figures that the atoms close to the drug are restricted in their movement, implying a drug-induced stiffening of DNA at this site in the simulated as well as the experimental structure. In this analysis, only non-hydrogen base-pair atoms are included. The restricted mobility in the presence of the drug is also reflected in the overall rms deviations of the averaged structures from their respective starting structures. For the $DNA_{no\ dist}$, DNA_{dist}, and DNA_{ideal} simulations, the rms deviations are 3.58, 2.51, and 2.66 Å, respectively, and the rms deviations averaged over all atoms except those of the end base pairs and the counterions are 1.08, 0.67, and 0.93 Å, respectively. The largest deviations and rms values correspond to the structure without bound distamycin. The deviations of our average structures of DNA with and without distamycin from the corresponding X-ray structures in terms of rms values, considering only the non-hydrogen base-pair atoms of the base pairs 2–11 and 13–23, are given in Figure 4.

Figures 5 and 4 make it apparent that the neglect of the crystal environment in our simulations results in end-group motions considerably larger than the observed motions of the DNA segment. As a result, neither structural nor dynamical properties of the end groups are simulated in a satisfactory way. However, the center of the helix appears to be described fairly well, since it exhibits only small displacements from the X-ray structure and its mobilities are close to the observed ones. Since our investigation mostly concerns the drug–DNA interaction involving the center base pairs, the shortcomings of our simulation with regard to the segment end groups should not be serious.

The flexibility of the end groups also affects the propeller twist angles, discussed in Coll et al. (1987, 1989), in the simulated structures. In Table III, the propeller twists of the two central base pairs are listed. The calculation yields values that are similar to the observed ones.

An important result of our investigation is the observation that distamycin stabilizes the B-form of DNA. This finding is based on a comprison of the average structures. In the case of simulation DNA_{dist}, with bound distamycin, the initial DNA B-form remains largely intact, whereas in the case of simulation $DNA_{no\ dist}$, *without* bound distamycin, there is evidence for a transition from a B-DNA to an A-DNA form. Table

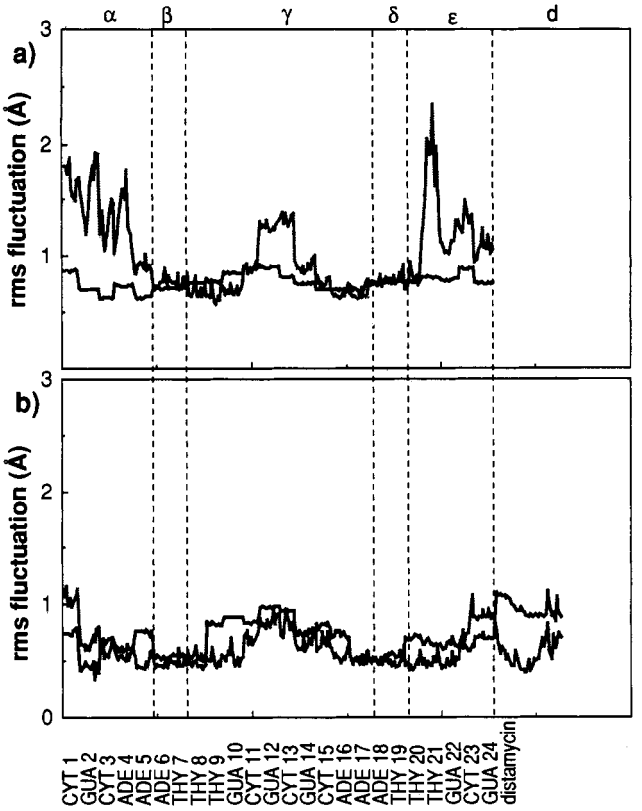

FIGURE 5: Mobilities of non-hydrogen base-pair atoms derived from the temperature factor of the X-ray analysis (black) and from the molecular dynamics simulation (gray) for the DNA segment without distamycin (simulation $DNA_{no\ dist}$) (a) and with distamycin (simulation DNA_{dist}) (b). The horizontal axis shows the base pair atoms. The following regions are identified: (α) CYT 1 to ADE 5; (β) central base pairs ADE 6 and THY 7; (γ) THY 8 to GUA 12 (helix a) and CYT 13 to ADE 17 (helix b); (δ) central base pairs ADE 18 and THY 19; (ϵ) THY 20 to GUA 24; and (d) distamycin.

Table IV: Comparison of Several Structural DNA Features[a]

DNA	minor groove (Å)	major groove (Å)	Ω (deg)	rms A (Å)	rms B (Å)
B	11.5	17.5	36.0		
A	16.8	8.5	32.7		
X-ray structure	9.6	19.4	35.7	5.5	1.1
$DNA_{no\ dist}$ (240)	16.3	11.4	33.7	3.2	3.7
$DNA_{no\ dist}$ (40)	15.9	10.0	33.5	3.0	4.2
DNA_{dist} (200)	11.8	17.6	37.7	5.4	2.5
DNA_{ideal} (200)	12.9	21.7	34.8	5.5	2.4

[a] The groove widths correspond to the average distances of the pertinent phosphorus atoms. The angle Ω measures the turn from one base pair to the next perpendicular to the main helix axis. The values given as typical for A- and B-type DNA have been taken from Saenger (1984). Ω in our average structures was calculated by CURVES2.1 (Lavery & Sklenar, 1989). The rms values given indicate the average deviations of the structures from respective standard A- and B-DNA's of Arnott and Hukins (1972). These values correspond to groove widths averaged (as indicated) over the final 240, 200, or 40 ps of the pertinent trajectories. The X-ray structure is from Coll et al. (1987).

IV lists some structural parameters typically found in A- and B-DNA (Saenger, 1984) as well as values taken from the simulations. One can see that in the case of the $DNA_{no\ dist}$ structures a transition from structural features close to B-DNA to features close to A-DNA takes place. Such a transition is not apparent in the cases of the DNA_{dist} and DNA_{ideal} simulations, both of which include distamycin bound in the minor groove.

The groove widths, measured by distances between nearest phosphorus atoms across the minor and the major grooves, of

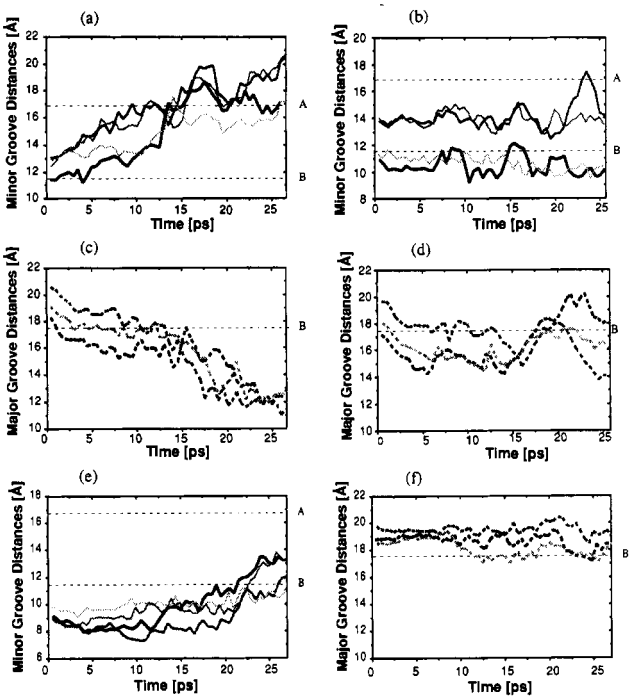

FIGURE 6: Groove widths, i.e., selected phosphorus–phosphorus distances across minor grooves (P8–P21, black; P10–P19, dark gray; P9–P20, medium gray; P7–P22, light gray) and major grooves (P17–P3, black dashed; P15–P5, gray dashed; P16–P4, light gray dashed), during the heating (first 12 ps) and equilibration (final 15 ps) phases of simulations $DNA_{no\ dist}$ (a and c), DNA_{dist} (b and d), and DNA_{water} (e and f). The values of the groove widths corresponding to DNA in the A-form and in the B-form are indicated by short dashes.

the DNA_{dist} and $DNA_{no\ dist}$ simulations during the initial 27 ps (12 ps of heating and 15 ps of equilibration) after minimization are provided in Figure 6, parts a–d. It is evident from these results that, in case of the $DNA_{no\ dist}$ simulation, the minor groove widens from distances normally found in B-DNA to those normally found in A-DNA. At the same time, the width of the major groove clearly decreases, another sign of a transition from the B- to the A-form. This trend toward an A-DNA conformation continues during the later 235 ps of the $DNA_{no\ dist}$ simulation. No such structural transitions are observed in any of the simulations with bound distamycin, as is evident from Figure 6. The groove widths of the DNA_{dist} system plotted in Figure 6 are, in fact, remarkably stable, even during the long 250-ps simulations.

It may be objected at this point that the transition from the B-form to the A-form in the case of simulation $DNA_{no\ dist}$ is due to our choice of the initial DNA geometry, namely the X-ray structure (Coll et al., 1987). Therefore, we carried out a short simulation (12 ps of heating and 15 ps of equilibration) on the standard DNA_{ideal} structure *without* bound distamycin. The resulting groove widths were found to develop in a way similar to that of the $DNA_{no\ dist}$ simulation, that is, a rapid transformation from goove widths corresponding to B-DNA to those corresponding to A-DNA occurred. We can thus state that the binding of distamycin in the minor groove prevents, or at least delays by more than 250 ps, the conformational changes observed in the simulated B-DNA.

It must be noted at this point that DNA under physiological conditions, i.e., in water, remains in the B-form. Our simulations, lacking external water, may not allow the conclusion that distamycin binding stabilizes the B-DNA geometry, since the simulations may be incapable of describing DNA geometries correctly. To address this critique, we carried out the simulation DNA_{water} defined above. Since it is known that

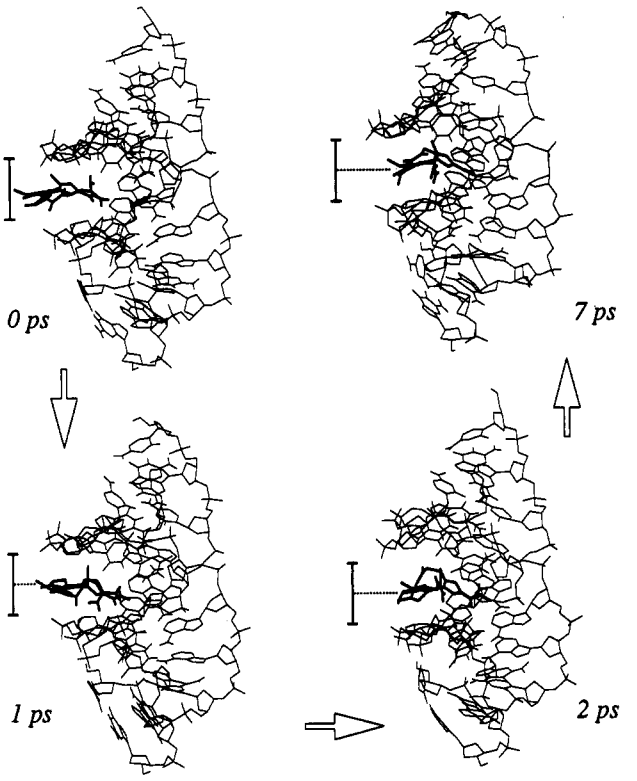

FIGURE 7: Side view of the minor groove during reentry of distamycin. Shown are four conformations, beginning at the upper left with a structure depicting the starting configuration of the simulation with distamycin moved out of the groove by a distance of approximately 4 Å. The vertical bar serves as a visual aid indicating the starting position of the drug.

the B-form of DNA is stable in water but not under dehydration, the simulations should predict a transition from the B-form to the A-form for the water-free systems, i.e., in the cases of the DNA_{dist} and DNA_{ideal} simulations, but should not yield such a transition when water is added as in the case of the DNA_{water} simulation.

In fact, this behavior has been observed by us, albeit only for the short simulation time of 27 ps, and is illustrated in Figure 6 parts e and f. Groove widths indicate that the B-DNA form is stable during the entire simulation period. As mentioned in the Methods section, a previous study by van Gunsteren et al. (1986) found the onset of a transition even in the presence of water, namely, a hybrid of about 30% A-DNA and 70% B-DNA, after a simulation of over 80 ps.

Distamycin Binding

In this section we investigate the dynamic aspects of the binding of distamycin to DNA. For this purpose we carried out the three simulations $DNA_{move\,1}$–$DNA_{move\,3}$ in which we initially moved distamycin from its position in the equilibrated DNA–distamycin complex to a new starting position. We then monitored the structure and distamycin–DNA interaction energies during the rebinding of distamycin.

Radial Displacement. In simulation $DNA_{move\,1}$, distamycin was moved out of the minor groove in a direction perpendicular to the helix axis, i.e., in radial direction, by a distance of approximately 4.1 Å. Two counterions close to the minor groove were moved outward in the same direction by small distances. After a brief minimization as described in the Methods section, the DNA–distamycin system was simulated for 60 ps. Four "snapshots" of the simulation depicting the position of distamycin in the minor groove are shown in Figure 7. The corresponding nonbonded energies between distamycin and the DNA segment are shown in Figure 8b. According to our simulation, distamycin returned to its original position in the equilibrated complex after only 7 ps. After 15–20 ps, the interaction energies between distamycin and the DNA strand are again largely similar to those of the equilibrated complex (Figure 8a).

From simulation $DNA_{move\,1}$, we can conclude that rebinding to distamycin, at least in a water-free environment and when the drug is sufficiently near the binding site (<5.0 Å), occurs very rapidly (20 ps) and selects the binding site of the X-ray structure. The binding energy has significant van der Waals and electrostatic contributions.

Movement along the Groove. Distamycin is known to bind in AT-rich DNA regions (Zimmer & Wahnert, 1986; Wang & Teng, 1990). The DNA sequence investigated in our study, d(CGCAAATTTGCG), has such a region at its center. The crystal structure (Coll et al., 1987) and the equilibrated DNA–distamycin complex show distamycin bound to the AAAT part of the sequence. In order to investigate the propensity for distamycin's binding at this position, we carried

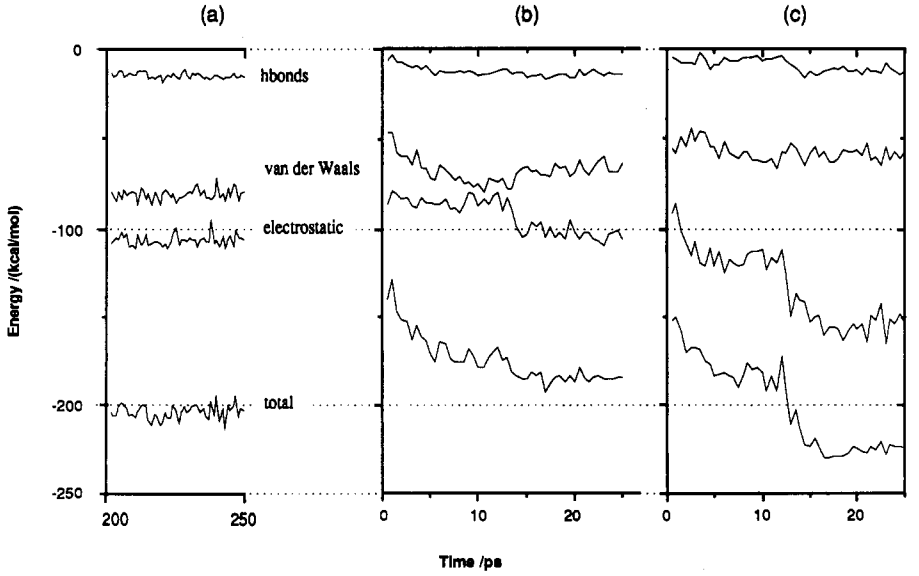

FIGURE 8: Comparison of the nonbonded energies between the DNA helix and distamycin during the latter part of the 250-ps simulation (a), during reentry into the minor groove (b), and in the major groove (c).

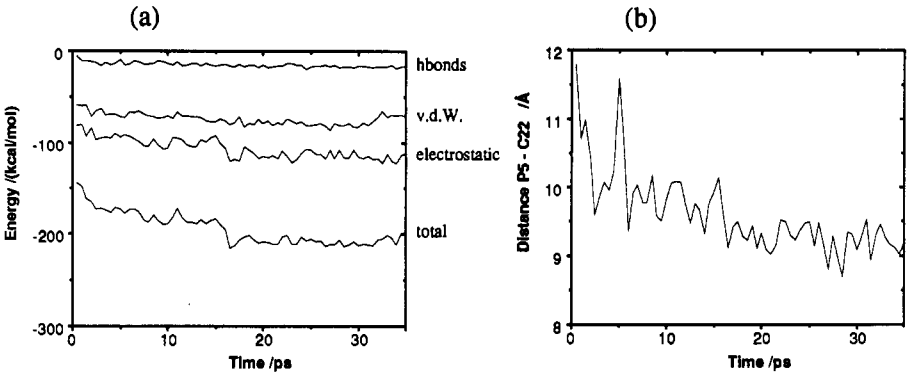

FIGURE 9: Nonbonded interaction energies between DNA and distamycin during the movement along the minor groove (a) and the distance between distamycin and phosphorus P5 of the DNA backbone (b).

out simulation $DNA_{move\,2}$ in which distamycin was initially moved two base pairs down the minor groove, i.e., to ATTT. During the simulation, distamycin moves up by one base pair into the AATT part of the sequence within ≈15–20 ps.

The interaction energies between distamycin and the DNA strand during simulation $DNA_{move\,2}$ are shown in Figure 9a. One can note a decrease of all three energy contributions (electrostatic, van der Waals, hydrogen bonding) during the initial 15–20 ps of simulation. During this period, distamycin moves up the minor groove in the direction of the original position. The motion is represented in some detail in Figure 9b, where the distance of atom C22 of distamycin to DNA backbone phosphorus atom P5 is presented as a function of time. It is evident that the position of distamycin stabilizes at approximately 15–20 ps after a movement of about 2.5 Å, i.e., a movement by one base pair. A comparison of the energies in Figure 9a with the corresponding energies of the equilibrated complex shown in Figure 8a reveals that distamycin is energetically near equilibrium. Longer simulations may reveal that distamycin can move further up the segment; however, it appears plausible that the time scale required for this motion could exceed the time scale feasible for molecular dynamics simulations (a few hundred picoseconds). It is of interest to note that NMR experiments (Klevit et al., 1986; Leupin et al., 1986; Wang et al., 1989) reveal a flip-flop mechanism of the binding of minor groove binding compounds, including distamycin, to the DNA double helix. However, the time scale of microseconds–nanoseconds observed by these experiments currently cannot be covered by molecular dynamics calculations.

Distamycin in the Major Groove. Distamycin binds in a specific manner to AT-rich sequences in the minor groove of DNA. We wanted to investigate if the preference for minor groove binding is also borne out by molecular dynamics simulations. For this purpose we carried out a 70-ps simulation $DNA_{move\,3}$ with a starting structure in which distamycin was placed in the major groove. This was done interactively with the use of Quanta (Polygen Corp., 1988), by the rotation of the distamycin 180° about the helix axis and the positioning of the drug on the opposite side of the strand in the major groove. The positively charged guanidinium end of distamycin (atoms N8 and N9 in Figure 2c) was placed between the phosphate groups of residues 3 and 19; the other end of the molecule was placed between the phosphate groups of residues 6 and 15. Subsequently, a 70-ps dynamics simulation was performed.

The nonbonded interaction energies between distamycin and the DNA strand in the major groove are shown in Figure 8c. A comparison with the corresponding energies in the minor groove (Figure 8 parts a and b) shows that van der Waals contributions favor binding in the minor groove. This can be readily understood by the fact that the drug fits "snuggly" in the minor groove (Pelton & Wemmer, 1988), as is apparent in Figure 1. A surprising aspect of Figure 8c is that the electrostatic contributions favor binding in the major groove by such a large measure that distamycin would preferably bind there, as is expressed by the total energies.

A detailed analysis of the trajectory shows that the drug changes its conformation during the 12–13-ps interval, i.e., when a sharp drop in the electrostatic energy occurs in Figure 8c. At this instance, the positive guanidinium end of the drug twists with respect to the remaining distamycin moiety and approaches one side of the major groove, in effect bridging the two phosphate groups P18 and P19. This position of distamycin is favored electrostatically because of the highly charged nature of the interacting groups.

The stability of distamycin in the major groove is at odds with the observation that distamycin binds mainly in the minor groove of DNA. This discrepancy is likely due to the neglect of water in our simulation. In fact, the equilibrated DNA–water system of DNA_{water} shows that water, initially deposited largely outside the DNA, is attracted into the major groove and, among other configurations, forms clusters around the DNA phosphorus atoms. For example, P19 is surrounded by 10 water molecules within a hydration shell of 5.0 Å. A detailed molecular dynamics analysis of DNA hydration and water dynamics can be found in earlier work by van Gunsteren et al. (1986) in which an average of 2.3 DNA–water hydrogen bonds were observed within a hydration shell of 4 Å of the phosphate oxygens. The authors state that these oxygens show 3 times more hydrogen bonding in their simulations than other oxygen atoms in DNA. We conclude, therefore, that preferred binding of distamycin in the major groove, as observed in $DNA_{move\,3}$, is prevented by tightly bound water molecules at the phosphate groups. Figure 8 shows that major groove energies prior to the electrostatic binding are equal to or larger than those in the minor groove. Because of the large number of water molecules observed in both grooves, DNA–drug binding is expected to be influenced by entropic effects as well.

SUMMARY

Several interesting conclusions have emerged from our simulations on DNA–distamycin binding. Foremost is the realization that distamycin binding induces a stiffening of the DNA helix and stabilization of the B-form. This conclusion follows from the reduction of rms amplitudes of atomic mobilities upon binding and from the fact that simulations without the drug show a transition to the A-form except if water is present. No such transition is observed for DNA–distamycin complexes. The mechanism for the prevention of this transition

appears to be the shape of the drug and its tight fit in the minor groove. Hydration shells around the phosphate groups appear to be partly responsible for distamycin's propensity to minor groove binding; major groove binding requires replacement of water in these shells since the guanidinium end of the drug seeks to move into the interstitial space between neighboring phosphate groups that is occupied by water.

Several important issues cannot be addressed in the present study due to the fact that only a very short DNA segment (12 base pairs) was investigated, the fact that the neglect of the crystal field in the simulation prevented a detailed comparison with the observed X-ray structure—in fact, one of our simulated systems changed to the A-form, and the fact that water could not be included with distamycin to study binding properties. This prevented us from addressing the question of why distamycin prefers AT-rich segments of DNA—base pairs other than AT were present only at the ends of the segment, which showed unusually large flexibilities.

Finally, simulations of larger DNA segments including external water, describing DNA–protein complexes, and covering longer simulation times are urgently needed. Simulation times below 1 ns are too brief to reproduce water replacement during drug binding and to allow sliding of the drug along the minor groove to take place. Also, the binding motif of regulatory proteins involving the major groove and structural implications, like stiffening or unwinding of the DNA strand, need to be studied. The present investigation along with the previous studies by others has shown promise in that DNA and molecular complexes with DNA can be described by molecular dynamics. One can expect that the methods of molecular modeling and molecular dynamics will prove useful when they can be scaled up to simulate much larger systems. This will require considerable advancements in computer hardware and programming. In this respect the emergence of massive parallel computers and their use for molecular dynamics simulations (Heller et al., 1990; Windemuth & Schulten, 1990) appear most promising and should open the study of the mechanisms of the control of gene expression.

Acknowledgments

We thank H. Treutlein and M. Tesch for very helpful advice, B. Walberer for his program MODEL, and R. Ahlrichs and M. Häser for their program DSCF.

References

Arnott, S., & Hukins, D. (1972) *Biochem. Biophys. Res. Commun. 47*, 1504–1507.

Berendsen, H. J. C., Postma, J. P. M., van Gunsteren, W. F., DiNola, A., & Haak, J. R. (1984) *J. Chem. Phys. 81*, 3684–3690.

Berkowitz, M., & McCammon, J. A. (1982) *Chem. Phys. Lett. 90*, 215.

Brooks, B. R., Bruccoleri, R. E., Olafson, B. D., States, D. J., Swaminathan, S., & Karplus, M. (1983) *J. Comput. Chem. 4*, 187–217.

Brooks, C. L., Brünger, A., & Karplus, M. (1985) *Biopolymers 24*, 843.

Brünger, A. T. (1988) X-PLOR, The Howard Hughes Medical Institute and Department of Molecular Biophysics and Biochemistry, Yale University, New Haven, CT.

Coll, M., Frederick, C. A., Wang, A. H.-J., & Rich, A. (1987) *Proc. Natl. Acad. Sci. U.S.A. 84*, 8385–8389.

Coll, M., Aymami, J., van der Marel, G. A., van Boom, J. H., Rich, A., & Wang, A. H.-J. (1989) *Biochemistry 28*, 310.

Creighton, S., Rudolph, B., Lybrand, T., Singh, U. C., Shafer, R., Brown, S., Kollman, P., Case, D. A., & Andrea, T. (1989) *J. Biomol. Struct. Dyn. 6*, 929–969.

Davidson, E. R. (1967) *J. Chem. Phys. 46*, 3320.

Dewar, M. J. S., & Thiel, W. (1977) *J. Am. Chem. Soc. 99*, 4899.

Dewar, M. J. S., Zoebisch, E. G., Healy, E. F., & Stewart, J. J. P. (1985) *J. Am. Chem. Soc. 107*, 3902.

Feuerstein, B. G., Pattabiraman, N., & Marton, L. J. (1989) *Nucleic Acids Res. 17*, 6883–6892.

Häser, M., & Ahlrichs, R. (1989) *J. Comput. Chem. 10*, 104.

Heinzmann, R., & Ahlrichs, R. (1976) *Theor. Chim. Acta 42*, 33.

Heller, H., Grubmüller, H., & Schulten, K. (1990) *Molecular Simulation 5*, 133–165.

Hurley, L. H. (1989) *J. Med. Chem. 32*, 2027–2033.

Huzinaga, S. (1971) *Approximate Atomic Functions*, Vol. 1, University of Alberta, Edmonton.

Huzinaga, S., Andzelm, J., Klobukowski, M., Radzio-Andzelm, E., Sakai, Y., & Tatewaki, H. (1984) *Gaussian Basis Sets for Molecular Calculations*, Elsevier, Amsterdam.

Klevit, R., Wemmer, D., & Reid, B. (1986) *Biochemistry 25*, 3296–3303.

Lavery, R., & Sklenar, H. (1989) CURVES, Laboratoire de Biochemie Théorique CNRS, Institut de Biologie Physico-Chimique, 13 rue Pierre et Marie Curie, Paris.

Leupin, W., Chazin, W. J., Hyberts, S., Denny, W. A., & Wuthrich, K. (1986) *Biochemistry 25*, 5902–5910.

Levitt, M. (1983) *Cold Spring Harbor Symp. Quant. Biol. 47*, 251–261.

Mulliken, R. A. (1955) *J. Chem. Phys. 23*, 1833.

Nilsson, L., & Karplus, M. (1986) *J. Comput. Chem. 7*, 591–616.

Pelton, J. G., & Wemmer, D. E. (1988) *Biochemistry 27*, 8088–8096.

Polygen Corp. (1988) Quanta, Polygen Corp., 200 Fifth Ave., Waltham, MA 02254.

Pople, J. A., Beveridge, D. L., & Dobosh, P. A. (1967) *J. Chem. Phys. 47*, 2026.

Powell, M. J. D. (1977) *Mathematical Programming 12*, 241–254.

Ptashne, M. (1986) *A Genetic Switch*, Cell Press and Blackwell Scientific Publications, Palo Alto, CA.

Ravishanker, G., Swaminathan, S., Beveridge, D. L., Lavery, R., & Sklenar, H. (1989) *J. Biomol. Struct. Dyn. 6*, 669–699.

Roby, K. R. (1974) *Mol. Phys. 27*, 81.

Saenger, W. (1984) *Principles of Nucleic Acid Structure*, Springer-Verlag, New York.

Singh, U. C., Weiner, S. J., & Kollman, P. (1985) *Proc. Natl. Acad. Sci. U.S.A. 82*, 755–759.

Smeyers, Y. G., Randez, J. J., Randez, F. J., Haro-Ruiz, M. D., & Hernandez-Laguna, A. (1988) *J. Mol. Struct.: THEOCHEM* 166, 141–146.

Stryer, L. (1988) *Biochemistry*, W. H. Freeman and Co., New York.

Tesch, M., & Schulten, K. (1990) *Chem. Phys. Lett. 169*, 97–102.

Tidor, B., Irikura, K. K., Brooks, B. R., & Karplus, M. (1983) *J. Biomol. Struct. Dyn. 1*, 231–252.

van Gunsteren, W. F., & Berendsen, H. J. C. (1977) *Mol. Phys. 34*, 1311.

van Gunsteren, W. F., Berendsen, H. J. C., Geurtsen, R. G., & Zwinderman, H. R. J. (1986) *Ann. N.Y. Acad. Sci. 482*, 287–303.
Walberer, B. (1990) Simulationen zur Faltung von Proteinen, Master's Thesis, Technische Universität München.
Wang, A. H.-J., & Teng, M. K. (1990) *Crystallographic and Modeling Methods in Molecular Design* (Bugg, C. E., & Ealick, S. E., Eds.) pp 123–150, Springer-Verlag, New York.
Wang, A. H.-J., Cottens, S., Dervan, P. B., Yesinkowski, J. P., van der Marel, G. A., & van der Boom, J. H. (1989) *J. Biomol. Struct. Dyn. 7*, 101–117.
Weiner, S. J., Kollman, P. A., Nguyen, D. T., & Case, D. A. (1986) *J. Comput. Chem. 7*, 230–252.
Windemuth, A., & Schulten, K. (1990) *Molecular Simulation 5*, 353–361.
Wong, C. F., Zheng, C., & McCammon, J. A. (1989) *Biopolymers 154*, 151–154.
Zimmer, C., & Wahnert, U. (1986) *Prog. Biophys. Mol. Biol. 47*, 31–112.

Escherichia coli Glutaredoxin: Cloning and Overexpression, Thermodynamic Stability of the Oxidized and Reduced Forms, and Report of an N-Terminal Extended Species†

Victoria A. Sandberg, Betsy Kren, James A. Fuchs, and Clare Woodward*

Department of Biochemistry, University of Minnesota, St. Paul, Minnesota 55108

Received October 8, 1990; Revised Manuscript Received February 1, 1991

ABSTRACT: *Escherichia coli* glutaredoxin (MW 9700) catalyzes intracellular redox reactions utilizing a disulfide/dithiol enzymatic mechanism involving the active-site residues -Cys-Pro-Tyr-Cys-. It is functionally related to the thioredoxin family and is expected to share similar three-dimensional structure [Eklund, H., Cambillau, C., Sjöberg, B.-M., Holmgren, A., Jörnvall, H., Höög, J.-O., & Brändén, C.-I. (1984) *EMBO J. 3*, 1443–1449]. We constructed an overexpression system in which production of glutaredoxin is controlled by temperature-sensitive expression of the phage T7 promoter. In addition to glutaredoxin, a second gene product is observed; this species, which we call glutaredoxin N, is glutaredoxin extended by the sequence Met-Arg-Arg-Glu-Ile- at the N terminus. We have begun characterization of the structure and stability of the oxidized and reduced forms of glutaredoxin (grx-S_2 and grx-$(SH)_2$, respectively). Secondary structure calculated from CD data agrees with that predicted from the three-dimensional model of Eklund et al. The cooperative denaturation reactions of oxidized and reduced glutaredoxin were measured in temperature-induced and guanidine hydrochloride induced unfolding experiments. Surprisingly, oxidized and reduced glutaredoxins are very similar in stability. In heat-induced denaturation, monitored by CD, T_m is 55 and 57 °C for oxidized and reduced, respectively. In GuHCl denaturation, monitored by fluorescence, the midpoint denaturant concentrations are 2 M for both oxidized and reduced. It follows that the redox potentials of the disulfide bond are similar in unfolded and folded glutaredoxin. This is unexpected because in *E. coli* thioredoxin the oxidized form is far more stable than the reduced [Kelley, R. F., Shalongo, W., Jagannadham, M. V., & Stellwagen, E. (1987) *Biochemistry 26*, 1406–1411] and the redox potential of folded thioredoxin is significantly more negative than that of unfolded thioredoxin [Lin, T.-Y., & Kim, P. (1989) *Biochemistry 28*, 5282–5287].

Escherichia coli glutaredoxin is a small monomeric enzyme that catalyzes intracellular redox reactions by cyclic breakage and reformation of the disulfide bond between its active-site cysteines in the sequence -Cys-Pro-Tyr-Cys- (Fuchs, 1989; Holmgren, 1979a). It plays a central role in ribonucleotide reduction (Holmgren, 1976, 1979b; Kren et al., 1988) and sulfate reduction (Tsang, 1981; Kren et al., 1988). Glutaredoxin also has been shown to participate in reduction of methionine sulfoxide (Fuchs, 1977; Fuchs & Carlson, 1981) and protein disulfide linkages (Holmgren, 1979a).

Physical characterization of glutaredoxin has been limited by protein availability. We have cloned the gene for glutaredoxin and obtained abundant yields in an overexpression system. This permits us to undertake a study of glutaredoxin enzymology and folding thermodynamics, of which this is the first report. We are especially interested in comparisons between glutaredoxin and *E. coli* thioredoxin, a related redox protein with functional and structural similarity to glutaredoxin but with little sequence identity. *E. coli* thioredoxin (MW 11 700) contains a similar active-site sequence, -Cys-Gly-Pro-Cys-, and like glutaredoxin its only cysteine residues constitute the active site. Glutaredoxin is coupled to oxidation/reduction of glutathione, whereas thioredoxin redox activity is coupled to thioredoxin reductase. In both systems the

† This work is supported by grants from the University of Minnesota Industry–University Cooperative Research Center for Biocatalytic Processing, the University of Minnesota Graduate School, NIH GM40775 (for J.A.F. and B.K.), and NIH Molecular Biophysics Training Grant GM08277 (for V.A.S.).

* Author to whom correspondence should be addressed.

0006-2960/91/0430-5475$02.50/0